

# Exclusive diffractive bremsstrahlung of one and two photons at forward rapidities: possibilities for experimental studies in $pp$ collisions at the LHC

Piotr Lebiedowicz,<sup>1,\*</sup> Otto Nachtmann,<sup>2,†</sup> and Antoni Szczurek<sup>c1,§</sup>

<sup>1</sup>*Institute of Nuclear Physics Polish Academy of Sciences,  
Radzikowskiego 152, PL-31342 Kraków, Poland*

<sup>2</sup>*Institut für Theoretische Physik, Universität Heidelberg,  
Philosophenweg 16, D-69120 Heidelberg, Germany*

## Abstract

We evaluate the cross section for diffractive bremsstrahlung of a single photon in the  $pp \rightarrow pp\gamma$  reaction at high energies and at forward photon rapidities. Several differential distributions, for instance, in  $y$ ,  $k_\perp$  and  $\omega$ , the rapidity, the absolute value of the transverse momentum, and the energy of the photon, respectively, are presented. We compare the results for our “exact” model with two versions of soft-photon-approximations, SPA1 and SPA2, where the radiative amplitudes contain only the leading terms proportional to  $\omega^{-1}$ . The SPA1, which does not have the correct energy-momentum relations, performs surprisingly well in the kinematic range considered. We discuss also azimuthal correlations between outgoing particles. The azimuthal distributions are not isotropic and are different for our exact model and SPAs. We discuss also the possibility of a measurement of two-photon-bremsstrahlung in the  $pp \rightarrow pp\gamma\gamma$  reaction. In our calculations we impose a cut on the relative energy loss ( $0.02 < \xi_i < 0.1$ ,  $i = 1, 2$ ) of the protons where measurements by the ATLAS Forward Proton (AFP) detectors are possible. The AFP requirement for both diffractively scattered protons and one forward photon (measured at LHCf) reduces the cross section for  $pp \rightarrow pp\gamma$  almost to zero. On the other hand, much less cross-section reduction occurs for  $pp \rightarrow pp\gamma\gamma$  when photons are emitted in opposite sides of the ATLAS interaction point and can be measured by two different arms of LHCf. For the SPA1 ansatz we find  $\sigma(pp \rightarrow pp\gamma\gamma) \simeq 0.03$  nb at  $\sqrt{s} = 13$  TeV and with the cuts  $0.02 < \xi_i < 0.1$ ,  $8.5 < y_3 < 9$ ,  $-9 < y_4 < -8.5$ . Our predictions can be verified by ATLAS and LHCf combined experiments.

<sup>c</sup> Also at College of Natural Sciences, Institute of Physics, University of Rzeszów, ul. Pigonia 1, PL-35310 Rzeszów, Poland.

<sup>\*</sup> Piotr.Lebiedowicz@ifj.edu.pl

<sup>†</sup> O.Nachtmann@thphys.uni-heidelberg.de

<sup>§</sup> Antoni.Szczurek@ifj.edu.pl

## I. INTRODUCTION

Bremsstrahlung of photons in nucleon-nucleon collisions is one of the basic processes in physics. It was extensively studied in the  $pp \rightarrow pp\gamma$  reaction at relatively small c.m. energies where the meson exchanges are responsible for the underlying  $pp$  interaction; see e.g. [1, 2]. In [1] also the two-photon bremsstrahlung in  $pp$  scattering was considered. The virtual-photon bremsstrahlung in the reactions  $NN \rightarrow NN(\gamma^* \rightarrow \ell^+\ell^-)$  was discussed in [3, 4].

At high energies, the  $pp \rightarrow pp\gamma$  reaction has not yet been measured. However, some feasibility studies of the measurement of the exclusive diffractive bremsstrahlung cross sections were performed for RHIC energies [5] and for LHC energies using the ATLAS forward detectors [6, 7].

In contrast, the inclusive differential production cross-section of forward photons in  $pp$  collisions was measured at  $\sqrt{s} = 510$  GeV with the RHICf detector (see [8]) and at  $\sqrt{s} = 0.9, 7$  and 13 TeV with the LHCf detector (see [9–11]). The LHCf experiment is designed to measure the photons emitted in the very forward rapidity region  $|y| > 8.4$ . In the ATLAS-LHCf combined analysis [12] the forward-photon spectra are measured by the LHCf detector, while the ATLAS inner tracker system is used to suppress non-diffractive events.<sup>1</sup> In addition, several joint analyses with ATLAS-LHCf are on-going; see the discussions in [13, 14].

In this Letter, we discuss exclusive diffractive photon bremsstrahlung in  $pp$  collisions for the LHC energy  $\sqrt{s} = 13$  TeV and at very-forward photon rapidities. We shall work within the tensor-pomeron model as proposed in [15] for soft hadronic high-energy reactions. The theoretical methods which we shall use in our present analysis were developed by us in [16, 17]. In [16] we discussed the soft-photon radiation in pion-pion scattering. Our standard, or also called by us “exact”, results for diffractive photon-bremsstrahlung were compared to various soft-photon approximations (SPAs). In [17] we extended these considerations to the  $pp \rightarrow pp\gamma$  reaction at  $\sqrt{s} = 13$  TeV, limiting ourselves to  $|y| < 5$  and  $1 \text{ MeV} < k_\perp < 100 \text{ MeV}$ . Here,  $k_\perp$  is the absolute value of the photon transverse momentum. Recently, in [18] we have discussed various central-exclusive production (CEP) processes of single photons. The CEP processes, for instance the photon-pomeron fusion, do not play an important role at forward photon rapidities and can be safely neglected there.

It is also worth noting that exclusive diffractive photon bremsstrahlung in high-energy  $pp$  collisions at forward rapidities was discussed earlier in [19–21] within somewhat different approaches. In general, the bremsstrahlung is not limited to photon production. The bremsstrahlung-type emission of  $\omega$  and  $\pi^0$  mesons in high-energy  $pp$  collisions was calculated in [22, 23].

An interesting proposal to study the forward production of “dark photons” via bremsstrahlung in  $pp$  collisions with the Forward Physics Facility at the High-Luminosity LHC was discussed recently in [24, 25].

Our Letter is organized as follows. In the next section, we discuss briefly the theoretical formalism. In Sec. II A we give analytic expressions for radiative amplitudes for the reaction  $pp \rightarrow pp\gamma$  for our “exact” and approximate approaches. In Sec. II B we discuss

<sup>1</sup> In this method, the preliminary photon energy spectrum has been obtained in two regions of photon rapidity ( $8.81 < y < 8.99$  and  $y > 10.94$ ), for events with no charged particles having  $p_t > 100 \text{ MeV}$  and  $|\eta| < 2.5$ , where  $\eta$  is the pseudorapidity.

two-photon bremsstrahlung in  $pp \rightarrow pp\gamma\gamma$ . We present our “exact” model results in Sec. III, along with comparisons to SPAs. Section IV contains our conclusions.

## II. THEORETICAL FORMALISM

### A. $pp \rightarrow pp\gamma$

We consider the reaction

$$p(p_a, \lambda_a) + p(p_b, \lambda_b) \rightarrow p(p'_1, \lambda_1) + p(p'_2, \lambda_2) + \gamma(k, \epsilon), \quad (2.1)$$

at high energies and small momentum transfers. The momenta are indicated in brackets, the helicities of the protons are denoted by  $\lambda_a, \lambda_b, \lambda_1, \lambda_2 \in \{1/2, -1/2\}$ , and  $\epsilon$  is the polarization vector of the photon. The energy-momentum conservation in (2.1) requires

$$p_a + p_b = p'_1 + p'_2 + k. \quad (2.2)$$

The kinematic variables are

$$\begin{aligned} s &= (p_a + p_b)^2 = (p'_1 + p'_2 + k)^2, \\ q_1 &= p_a - p'_1, \quad t_1 = q_1^2, \\ q_2 &= p_b - p'_2, \quad t_2 = q_2^2, \\ s_1 &= W_1^2 = (p'_1 + k)^2 = (p_a + q_2)^2, \\ s_2 &= W_2^2 = (p'_2 + k)^2 = (p_b + q_1)^2. \end{aligned} \quad (2.3)$$

In the following we work in the overall c.m. system where we choose the 3 axis in the direction of  $\mathbf{p}_a$  (the beam direction). The rapidity of the photon is then

$$y = \frac{1}{2} \ln \frac{k^0 + k^3}{k^0 - k^3} = \tanh^{-1} \left( \frac{k^3}{k^0} \right) = -\ln \tan \frac{\theta}{2}, \quad (2.4)$$

where  $\theta$  is the polar angle of  $\mathbf{k}$ ,  $\cos \theta = k^3/|\mathbf{k}|$ . For the energy  $k^0$  of the photon we use the notation  $\omega$ . We introduce the variables  $\xi_1$  and  $\xi_2$  which, to a very good approximation, describe the the fractional energy losses of the protons  $p(p_a)$  and  $p(p_b)$

$$\xi_1 = \frac{p_b \cdot q_1}{p_b \cdot p_a} = \frac{p_a^0 - p'_1{}^0}{p_a^0} + \mathcal{O} \left( \frac{M^2}{s} \right), \quad \xi_2 = \frac{p_a \cdot q_2}{p_a \cdot p_b} = \frac{p_b^0 - p'_2{}^0}{p_b^0} + \mathcal{O} \left( \frac{M^2}{s} \right). \quad (2.5)$$

Here the energies of the incoming and outgoing protons, respectively, are

$$p_a^0 = p_b^0 = \frac{\sqrt{s}}{2}, \quad (2.6)$$

$$p'_{1,2}{}^0 = \frac{1}{2\sqrt{s}}(s + m_p^2 - s_{2,1}), \quad (2.7)$$

and we set  $M^2 = \max(m_p^2, |t_1|, |t_2|, k_\perp^2)$ . Alternatively, the proton relative energy-loss parameters can be expressed by the kinematical variables of the photon,

$$\xi_1 = \frac{k_\perp}{\sqrt{s}} \exp(y) + \mathcal{O} \left( \frac{M^2}{s} \right), \quad \xi_2 = \frac{k_\perp}{\sqrt{s}} \exp(-y) + \mathcal{O} \left( \frac{M^2}{s} \right). \quad (2.8)$$

The cross section for the photon yield can be calculated as follows

$$d\sigma(pp \rightarrow pp\gamma) = \frac{1}{2\sqrt{s(s-4m_p^2)}} \frac{d^3k}{(2\pi)^3 2k^0} \int \frac{d^3p'_1}{(2\pi)^3 2p_1^0} \frac{d^3p'_2}{(2\pi)^3 2p_2^0} \\ \times (2\pi)^4 \delta^{(4)}(p'_1 + p'_2 + k - p_a - p_b) \frac{1}{4} \sum_{p \text{ spins}} \mathcal{M}_\mu \mathcal{M}_\nu^* (-g^{\mu\nu}); \quad (2.9)$$

see Eqs. (2.33)–(2.35) of [17].  $\mathcal{M}_\mu$  is the radiative amplitude.

The standard (exact) photon-bremsstrahlung amplitude,  $\mathcal{M}_\mu^{\text{standard}}$ , treated in the tensor-pomeron approach, see (2.62) and (B3) of [17], includes 6 diagrams shown in Fig. 3(a)–(f) of [17]. The amplitudes (a), (b), (d), and (e), corresponding to photon emission from the external protons, are determined by the off-shell  $pp$  elastic scattering amplitude. The contact terms, (c) and (f), are needed in order to satisfy gauge-invariance constraints. For details how to calculate these standard results, which we call also exact results, we refer the reader to Sec. II C and Appendix B of [17].

In the following, we shall compare our “exact” results to two soft-photon approximations, SPA1 and SPA2, as defined in Sec. III of [17]. In both SPAs we keep only the pole terms  $\propto \omega^{-1}$ . We consider only the pomeron-exchange contribution for the radiative amplitudes, the leading term at high energies. In a first approximation we neglect absorption effects due to proton-proton interactions.

In SPA1, the radiative amplitude has the form

$$\mathcal{M}_\mu \rightarrow \mathcal{M}_{\mu, \text{SPA1}} = e \mathcal{M}^{(\text{on shell}) pp}(s, t) \left[ -\frac{p_{a\mu}}{(p_a \cdot k)} + \frac{p_{1\mu}}{(p_1 \cdot k)} - \frac{p_{b\mu}}{(p_b \cdot k)} + \frac{p_{2\mu}}{(p_2 \cdot k)} \right], \quad (2.10)$$

where  $\mathcal{M}^{(\text{on shell}) pp}(s, t)$  is the amplitude for on-shell  $pp$ -scattering

$$p(p_a, \lambda_a) + p(p_b, \lambda_b) \rightarrow p(p_1, \lambda_1) + p(p_2, \lambda_2), \\ p_a + p_b = p_1 + p_2; \quad (2.11)$$

see (2.19) and (3.1) of [17]. The inclusive photon cross section for the SPA1 case is

$$d\sigma(pp \rightarrow pp\gamma)_{\text{SPA1}} = \frac{d^3k}{(2\pi)^3 2k^0} \int d^3p_1 d^3p_2 e^2 \frac{d\sigma(pp \rightarrow pp)}{d^3p_1 d^3p_2} \\ \times \left[ -\frac{p_{a\mu}}{(p_a \cdot k)} + \frac{p_{1\mu}}{(p_1 \cdot k)} - \frac{p_{b\mu}}{(p_b \cdot k)} + \frac{p_{2\mu}}{(p_2 \cdot k)} \right] \\ \times \left[ -\frac{p_{a\nu}}{(p_a \cdot k)} + \frac{p_{1\nu}}{(p_1 \cdot k)} - \frac{p_{b\nu}}{(p_b \cdot k)} + \frac{p_{2\nu}}{(p_2 \cdot k)} \right] (-g^{\mu\nu}). \quad (2.12)$$

Here

$$\frac{d\sigma(pp \rightarrow pp)}{d^3p_1 d^3p_2} = \frac{1}{2\sqrt{s(s-4m_p^2)}} \frac{1}{(2\pi)^3 2p_1^0 (2\pi)^3 2p_2^0} \\ \times (2\pi)^4 \delta^{(4)}(p_1 + p_2 - p_a - p_b) \frac{1}{4} \sum_{p \text{ spins}} |\mathcal{M}^{(\text{on shell}) pp}(s, t)|^2, \quad (2.13)$$

where we neglect the photon momentum  $k$  in the energy-momentum conserving  $\delta^{(4)}(\cdot)$  function. For SPA1 results we impose restrictions on the proton's relative energy loss variables  $\xi_i$  by using (2.8) neglecting terms of  $\mathcal{O}(M^2/s)$ .

In the SPA2 case, we keep the exact energy-momentum relation (2.2). Here we calculate the photon yield using (2.9) replacing the radiative amplitude as follows

$$\mathcal{M}_\mu \rightarrow \mathcal{M}_{\mu, \text{SPA2}} = \mathcal{M}_{\mathbb{P}, \mu}^{(a+b+c)1} + \mathcal{M}_{\mathbb{P}, \mu}^{(d+e+f)1}. \quad (2.14)$$

The explicit expressions of these terms are given by (3.4), (B4), and (B15) of [17].

## B. $pp \rightarrow pp\gamma\gamma$

Here we consider the reaction

$$p(p_a) + p(p_b) \rightarrow p(p'_1) + p(p'_2) + \gamma(k_3) + \gamma(k_4). \quad (2.15)$$

We shall study this reaction under specific conditions. We shall require that one photon is emitted at forward and one at backward rapidities,  $8.5 < y_3 < 9$  and  $-9 < y_4 < -8.5$ , respectively, and that  $0.02 < \xi_{1,2} < 0.1$ .<sup>2</sup>

For the calculation of the radiative amplitudes we use SPA1. Here in the  $2 \rightarrow 4$  kinematics for SPA1 we define

$$\begin{aligned} \xi_1 &= \frac{k_{\perp 3}}{\sqrt{s}} \exp(y_3) + \frac{k_{\perp 4}}{\sqrt{s}} \exp(y_4), \\ \xi_2 &= \frac{k_{\perp 3}}{\sqrt{s}} \exp(-y_3) + \frac{k_{\perp 4}}{\sqrt{s}} \exp(-y_4). \end{aligned} \quad (2.16)$$

We shall see below in Sec. III that, indeed, the above cuts on  $\xi_1$  and  $\xi_2$  assure that to a good approximation we can restrict ourselves to the diagrams shown in Fig. 1. Then, the two-photon bremsstrahlung amplitude has the form

$$\mathcal{M}_{\mu\nu, \text{SPA1}} = e^2 \mathcal{M}^{(\text{on shell}) pp}(s, t) \left[ -\frac{p_{a\mu}}{(p_a \cdot k_3)} + \frac{p_{1\mu}}{(p_1 \cdot k_3)} \right] \left[ -\frac{p_{b\nu}}{(p_b \cdot k_4)} + \frac{p_{2\nu}}{(p_2 \cdot k_4)} \right], \quad (2.17)$$

and the inclusive two-photon cross section is

$$\begin{aligned} d\sigma(pp \rightarrow pp\gamma\gamma)_{\text{SPA1}} &= \frac{d^3k_3}{(2\pi)^3 2k_3^0} \frac{d^3k_4}{(2\pi)^3 2k_4^0} \int d^3p_1 d^3p_2 e^4 \frac{d\sigma(pp \rightarrow pp)}{d^3p_1 d^3p_2} \\ &\times \left[ -\frac{p_{a\mu}}{(p_a \cdot k_3)} + \frac{p_{1\mu}}{(p_1 \cdot k_3)} \right] \left[ -\frac{p_{b\nu}}{(p_b \cdot k_4)} + \frac{p_{2\nu}}{(p_2 \cdot k_4)} \right] \\ &\times \left[ -\frac{p_{a\alpha}}{(p_a \cdot k_3)} + \frac{p_{1\alpha}}{(p_1 \cdot k_3)} \right] \left[ -\frac{p_{b\beta}}{(p_b \cdot k_4)} + \frac{p_{2\beta}}{(p_2 \cdot k_4)} \right] \\ &\times (-g^{\mu\alpha})(-g^{\nu\beta}). \end{aligned} \quad (2.18)$$

<sup>2</sup> The AFP acceptance is limited by  $\xi$  and transverse momentum  $p_{t,p}$  of the scattered protons; see Fig. 8 of [26].

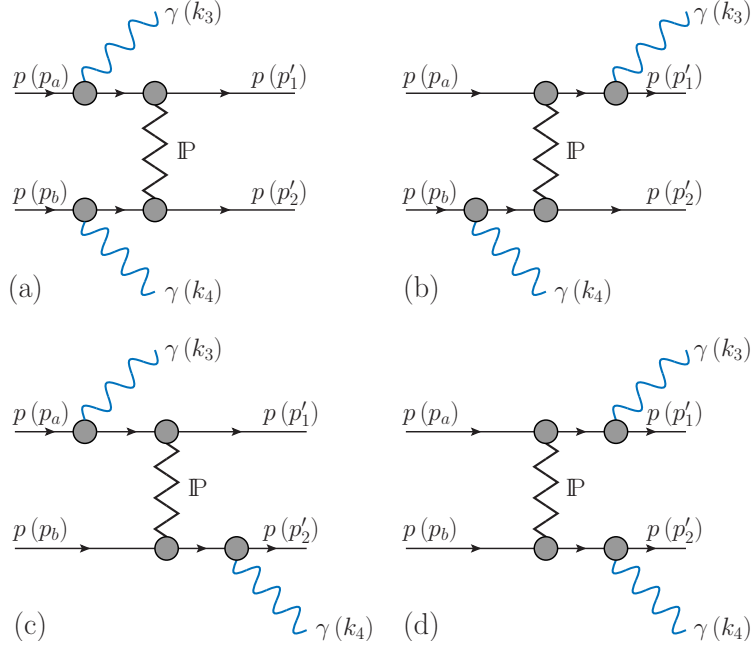


FIG. 1. Diffractive two-photon bremsstrahlung diagrams for the reaction  $pp \rightarrow pp\gamma\gamma$  (2.15) with exchange of the pomeron  $\mathbb{P}$ . These four diagrams (a – d) contribute to the SPA1 amplitude (2.17). In addition there are the diagrams where the two photons are emitted from the  $p_a$ - $p'_1$  line or from the  $p_b$ - $p'_2$  line, and various contact terms. These diagrams are not shown here.

### III. RESULTS

#### A. Single photon emission

In the following we consider explicitly only photon emission in very forward direction ( $y \gg 1$ ), where the photon is emitted predominantly from  $p(p_a)$  plus  $p(p'_1)$ ; see (2.1). As we see from (2.8) we have here  $\xi_1$  sizeable but  $\xi_2$  very small. In fact, then the proton  $p(p'_2)$ , having nearly the same energy as the incoming proton  $p(p_b)$ , cannot be measured by the present AFP detectors. Therefore, requiring for single emission that both final state protons are measured by the AFP detectors reduces the cross section essentially to zero. Thus, for photon emission at  $y \gg 1$  we consider only detection of  $p(p'_1)$  in the AFP detector. Of course, for  $y \ll -1$  the roles of  $p(p'_1)$  and  $p(p'_2)$  are interchanged and all distributions shown below for  $y \gg 1$  are easily transferred to  $y \ll -1$ .

In Fig. 2 we show the distributions in rapidity of the photon [see the panel (a)], in the absolute value of the transverse momentum of the photon [see the panel (b)], in  $\xi_1$  [see the panel (c)], and in the energy of the photon [see the panel (d)]. Shown are the results in the forward rapidity region for our exact model (or standard bremsstrahlung results) for the  $pp \rightarrow pp\gamma$  reaction together with the results obtained via SPA1 and SPA2 discussed in Sec. II A. We see from the panels (a) and (b) of Fig. 2 that bremsstrahlung photons are emitted predominantly in very forward-rapidity region  $9 < y < 10$  and with small values of  $k_\perp$ ; see also the left panel of Fig. 4 below. Forward photons will be measured by the LHCf experiment in the regions  $8.5 \lesssim y \lesssim 9$  and  $y \gtrsim 11$ . Due to the cut  $0.02 < \xi_1 < 0.1$  the energy of the photons is limited to  $120 \text{ GeV} < \omega < 660 \text{ GeV}$ ; see the panels (c) and (d)

of Fig. 2. Note, that due to the cuts specified in the figure legend the distributions in  $k_\perp$  and  $\omega$  have no singularity for  $k_\perp \rightarrow 0$ , respectively  $\omega \rightarrow 0$ . The  $k_\perp$  distribution reaches a maximum at  $k_\perp \sim 0.014$  GeV, and then it quickly decreases with increasing  $k_\perp$ .

In the SPA1, the photon momentum  $k$  was, on purpose, omitted in the energy-momentum conserving  $\delta$  function in the evaluation of the cross section [see (2.12) and (2.13)]. Here, the cross section is integrated over  $k_\perp$  from  $k_{\perp\min}$  to a maximal value  $k_{\perp\max}$  which we set to 1 GeV. In the SPA2, the correct  $2 \rightarrow 3$  kinematics is used. Recall that in both SPAs we keep only the pole terms  $\propto \omega^{-1}$  in the radiative amplitudes. We see from Fig. 2 that the SPA1, which does not have the correct energy-momentum relations, performs surprisingly well in the kinematic range considered. For the SPA2, the deviations from our exact (standard) result increase rapidly with growing  $k_\perp$  and  $\omega$ . From this comparison we see the importance of the interference between the pole term and the non-leading, but numerically large, terms occurring in the radiative amplitudes. It is essential to add coherently all the various parts of the amplitude for the bremsstrahlung-type emission of photons in order not to miss important interference effects. For more details on the size of various contributions we refer to the discussions in [17] (see, e.g., Fig. 17 there).

In the standard result, all contributions to the radiative amplitude with Dirac and Pauli terms are included. Figure 3 shows the complete (total) standard results and the results for Dirac and Pauli terms individually. The anomalous magnetic moment of the proton (Pauli term) plays an important role for larger values of  $k_\perp$  and  $\omega$ .

In Fig. 4 we show the two-dimensional differential cross sections in the  $k_\perp$ -y plane (left panel) and in the  $\omega$ -y plane (right panel) imposing a typical cut  $0.02 < \xi_1 < 0.1$  on the fractional energy loss of the ‘emitting’ proton.

In Fig. 5 we show the results for  $d\sigma/dk_\perp$  and  $d\sigma/d\omega$  for  $\sqrt{s} = 13$  TeV,  $0.02 < \xi_1 < 0.1$ , as in Figs. 2(b) and 2(d) but now for a more restrictive y cut,  $8.5 < y < 9$ . We see that the  $k_\perp$  and  $\omega$  distributions are reduced by a factor of order 10 compared to their counterparts in Figs. 2 (b) and (d). The kink at  $k_\perp \approx 0.17$  GeV is due to the cut on y.

In Fig. 6 we show the distributions in absolute value of the transverse momenta,  $p_{t,1}$  and  $p_{t,2}$ , of the outgoing protons  $p(p'_1)$  and  $p(p'_2)$ , see the solid and dashed lines, respectively. Results for two y intervals are shown:  $6 < y < 13$  (left panel) and  $8.5 < y < 9$  (right panel). One can see that the cross sections reach a maximum at  $p_{t,p} \sim \sqrt{|t_{1,2}|} \sim 0.25$  GeV and that  $d\sigma/dp_{t,1} \neq d\sigma/dp_{t,2}$ . We find that for  $p_{t,1} > 0.8$  GeV, the Pauli component gives a sizeable contribution.

Now we consider the azimuthal angles  $\phi_i$  of the transverse momenta of the protons  $p(p'_i)$  and the photon  $\gamma(k)$

$$\begin{aligned} p'_{i\perp} &= p_{t,i} e^{i\phi_i}, \quad (i = 1, 2), \\ k_\perp &= k_\perp e^{i\phi_3}, \\ 0 &\leq \phi_i < 2\pi, \quad (i = 1, 2, 3). \end{aligned} \tag{3.1}$$

Here the azimuth  $\phi = 0$  corresponds to some fixed transverse direction in the LHC system which is also the c.m. system for our reactions. Transverse-momentum conservation requires

$$p'_{1\perp} + p'_{2\perp} + k_\perp = 0. \tag{3.2}$$

Therefore, a measurement of  $p'_{1\perp}$  and  $k_\perp$  determines also  $p'_{2\perp}$ .

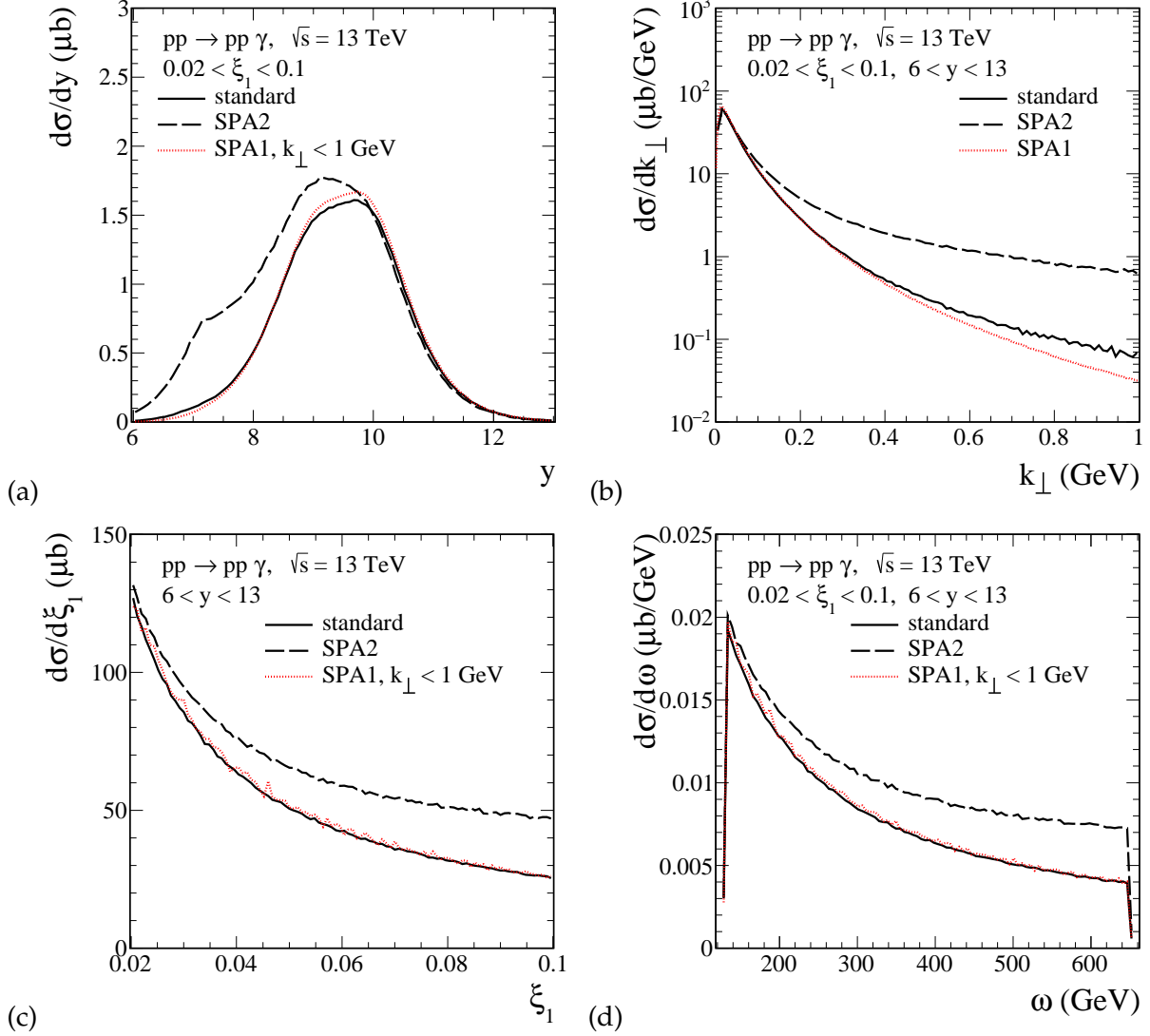


FIG. 2. The differential distributions in the rapidity of the photon (a), in the transverse momentum of the photon (b), in the energy-loss variable  $\xi_1$  (c), and in the energy of the photon (d) for the  $pp \rightarrow pp\gamma$  reaction via bremsstrahlung. The calculations were done for  $\sqrt{s} = 13$  TeV,  $6 < y < 13$ , and with the cut  $0.02 < \xi_1 < 0.1$ . For SPA1 an additional cut  $k_\perp < 1$  GeV was imposed. The solid line corresponds to our standard bremsstrahlung model, the black long-dashed line corresponds to SPA2 (2.14), and the red dotted line corresponds to SPA1 (2.10). The oscillations in the SPA1 results are of numerical origin

Figure 7 shows the distributions in  $\tilde{\phi}_{ij}$  defined as

$$\tilde{\phi}_{ij} = \phi_i - \phi_j \mod(2\pi), \quad (3.3)$$

where we require

$$0 \leq \tilde{\phi}_{ij} < 2\pi. \quad (3.4)$$

In the top panels of Fig. 7 we show the results in  $\tilde{\phi}_{12}$ , the angle between the transverse momenta of the outgoing protons, for our standard and SPA2 calculations. For SPA1



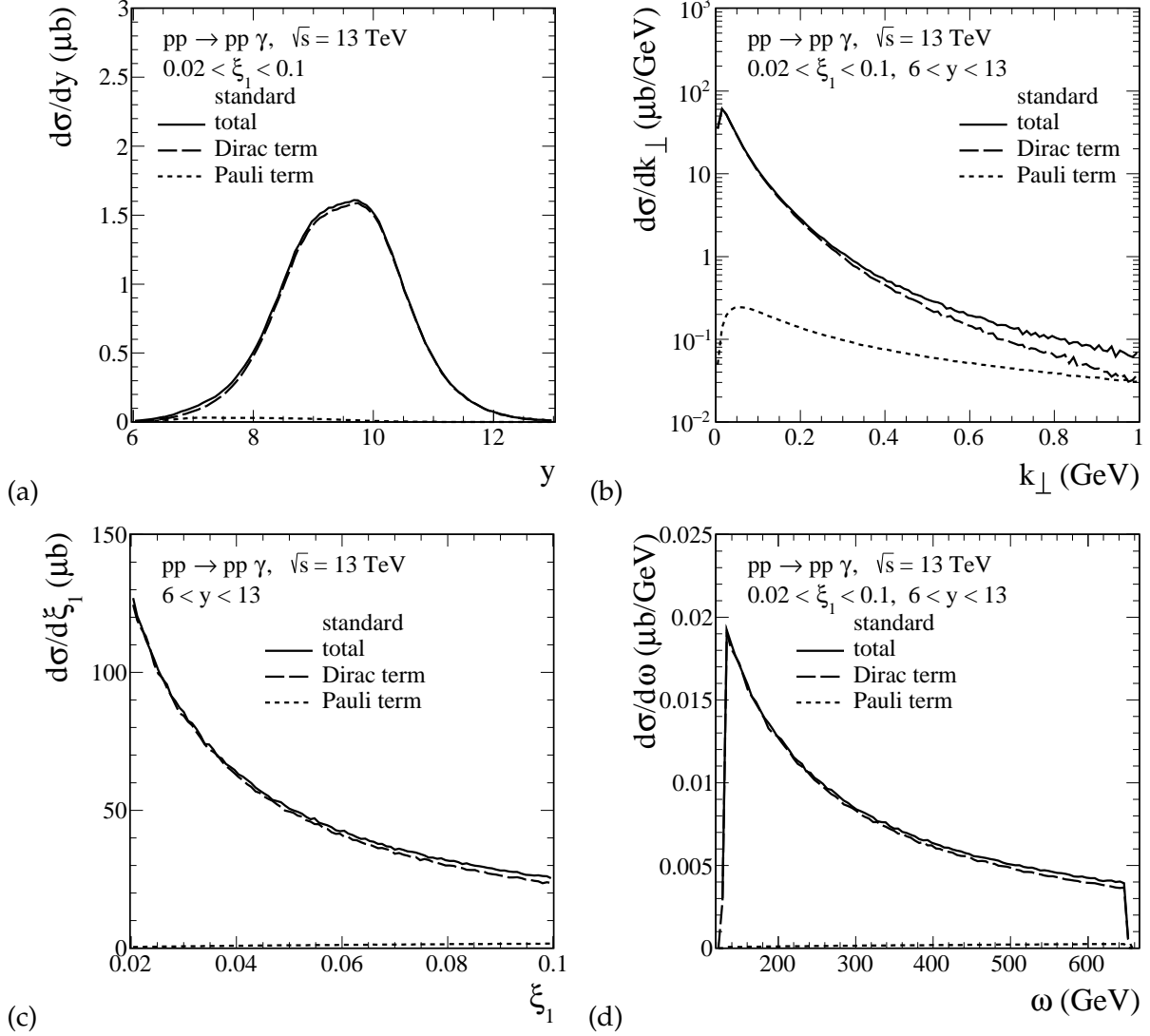


FIG. 3. The differential cross sections for the  $pp \rightarrow pp\gamma$  reaction via bremsstrahlung as in Fig. 2 but here shown are only standard complete results (total) and the results for the Dirac and Pauli terms alone.

(not shown here) the outgoing protons are back-to-back ( $\tilde{\phi}_{12} = \pi$ ). We see that also for our standard approach  $\tilde{\phi}_{12} \approx \pi$  gives the main contribution. That is, very roughly the outgoing protons and the beam are in one plane  $\mathcal{S}_0$ . The width of the distribution in  $\tilde{\phi}_{12}$  depends on the  $y$  cut with the more restrictive  $y$  cut (right panel) giving a wider distribution.

The bottom panels of Fig. 7 show the distributions in  $\tilde{\phi}_{13}$  ( $\tilde{\phi}_{23}$ ), the azimuthal angles between the proton  $p(p'_1)$  ( $p(p'_2)$ ) and  $\gamma(k)$ ; see Eq. (3.3). The SPA1 and our standard results show maxima for  $\tilde{\phi}_{13}$  and  $\tilde{\phi}_{23}$  around  $\pi/2$  and  $3\pi/2$ . This corresponds to emission of the photon in a plane  $\mathcal{S}_1$  which is orthogonal to the plane  $\mathcal{S}_0$  defined above. The SPA2 results for the  $\tilde{\phi}_{13}$  and  $\tilde{\phi}_{23}$  distributions deviate very significantly from our standard results.

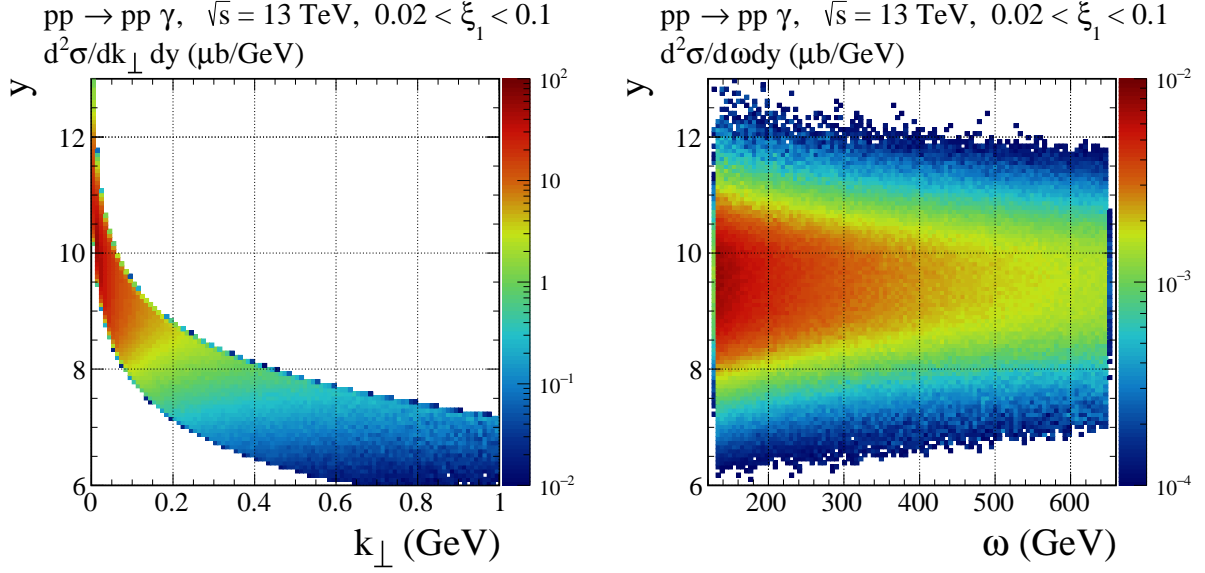


FIG. 4. The two-dimensional distributions in  $(k_\perp, y)$  and in  $(\omega, y)$  for the  $pp \rightarrow pp\gamma$  reaction for our standard bremsstrahlung model calculated for  $\sqrt{s} = 13$  TeV,  $6 < y < 13$ , and  $0.02 < \xi_1 < 0.1$ .

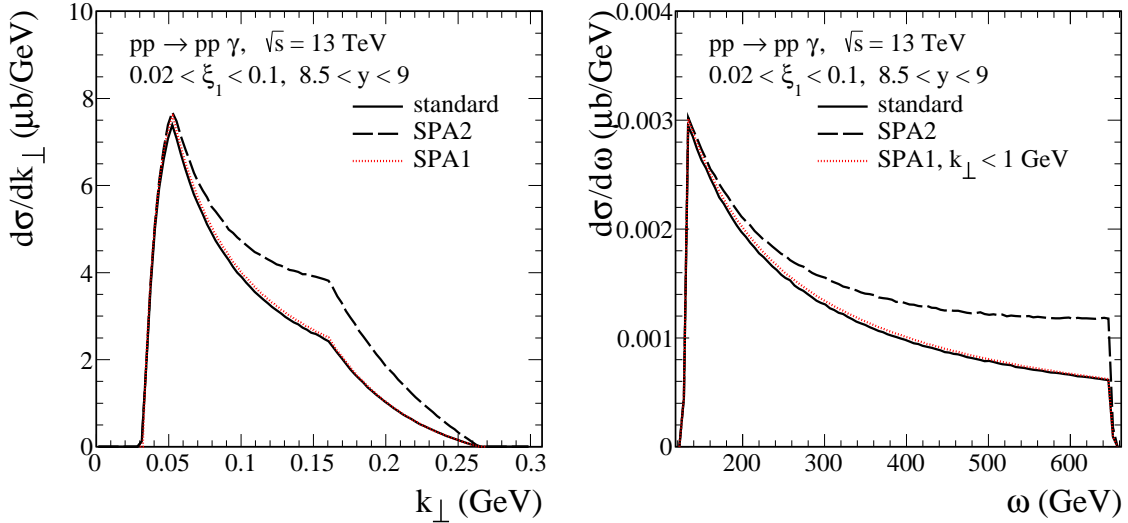


FIG. 5. The differential distributions in the transverse momentum of the photon (left) and in the energy of the photon (right) for the  $pp \rightarrow pp\gamma$  reaction. The calculations were done for  $\sqrt{s} = 13$  TeV,  $8.5 < y < 9$ , and  $0.02 < \xi_1 < 0.1$ . The meaning of the lines is the same as in Fig. 2.

## B. Results for emission of two photons

In Fig. 8 we show the results for the  $pp \rightarrow pp\gamma\gamma$  reaction, discussed in Sec. II B, calculated for  $\sqrt{s} = 13$  TeV and in the kinematic region specified in the figure caption. The shapes of distributions in the first four panels are analogous to the ones for single photon emission. The lowest panel shows azimuthal correlations between forward proton and forward photon (solid line) and between backward proton and backward photon (dashed

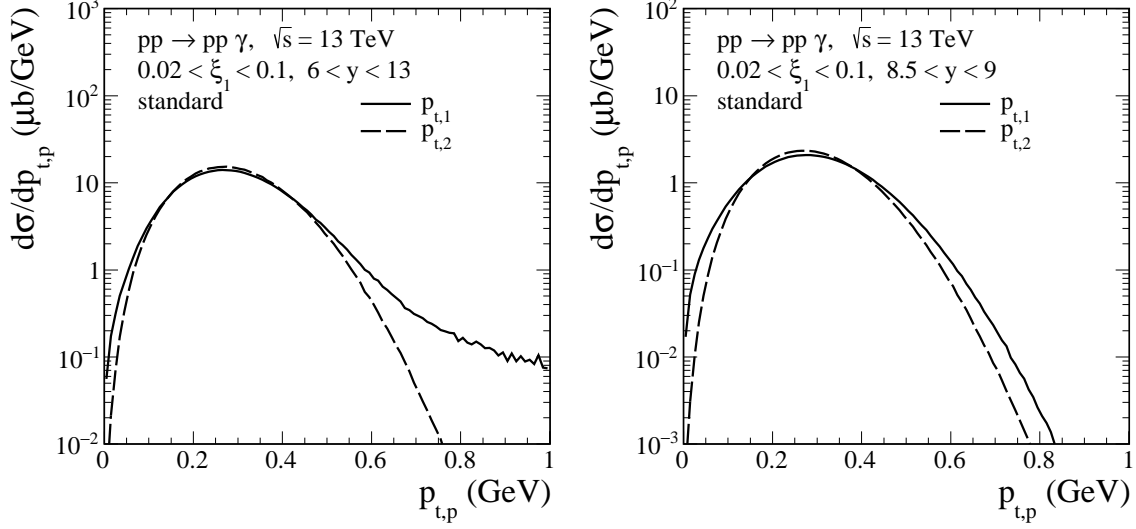


FIG. 6. The distributions in the absolute values of the transverse momenta of the outgoing protons for the  $pp \rightarrow pp\gamma$  reaction calculated for  $\sqrt{s} = 13$  TeV,  $0.02 < \xi_1 < 0.1$ ,  $6 < y < 13$  (left panel), and  $8.5 < y < 9$  (right panel). The solid (dashed) line, denoted as  $p_{t,1}$  ( $p_{t,2}$ ), corresponds to the proton  $p(p'_1)$  ( $p(p'_2)$ ).

line). The fact of seemingly different distributions for forward and backward emissions is due to the way how the azimuthal angles are defined in (3.1) and (3.3) which leads to the symmetry relation

$$\frac{d\sigma^{\text{backward}}}{d\phi}(\phi) = \begin{cases} \frac{d\sigma^{\text{forward}}}{d\phi}(\phi + \pi) & \text{for } 0 \leq \phi < \pi, \\ \frac{d\sigma^{\text{forward}}}{d\phi}(\phi - \pi) & \text{for } \pi \leq \phi < 2\pi. \end{cases} \quad (3.5)$$

This explains the observed differences between the solid and dashed lines.

Finally we note that emission of the two photons either from the  $p_a-p'_1$  line or from the  $p_b-p'_2$  line in Fig. 1 should essentially not contribute to the distributions shown in Fig. 8. Such processes will give two photons on one side of the interaction point and the final proton on the opposite side will miss the  $\zeta$  cut which we impose.

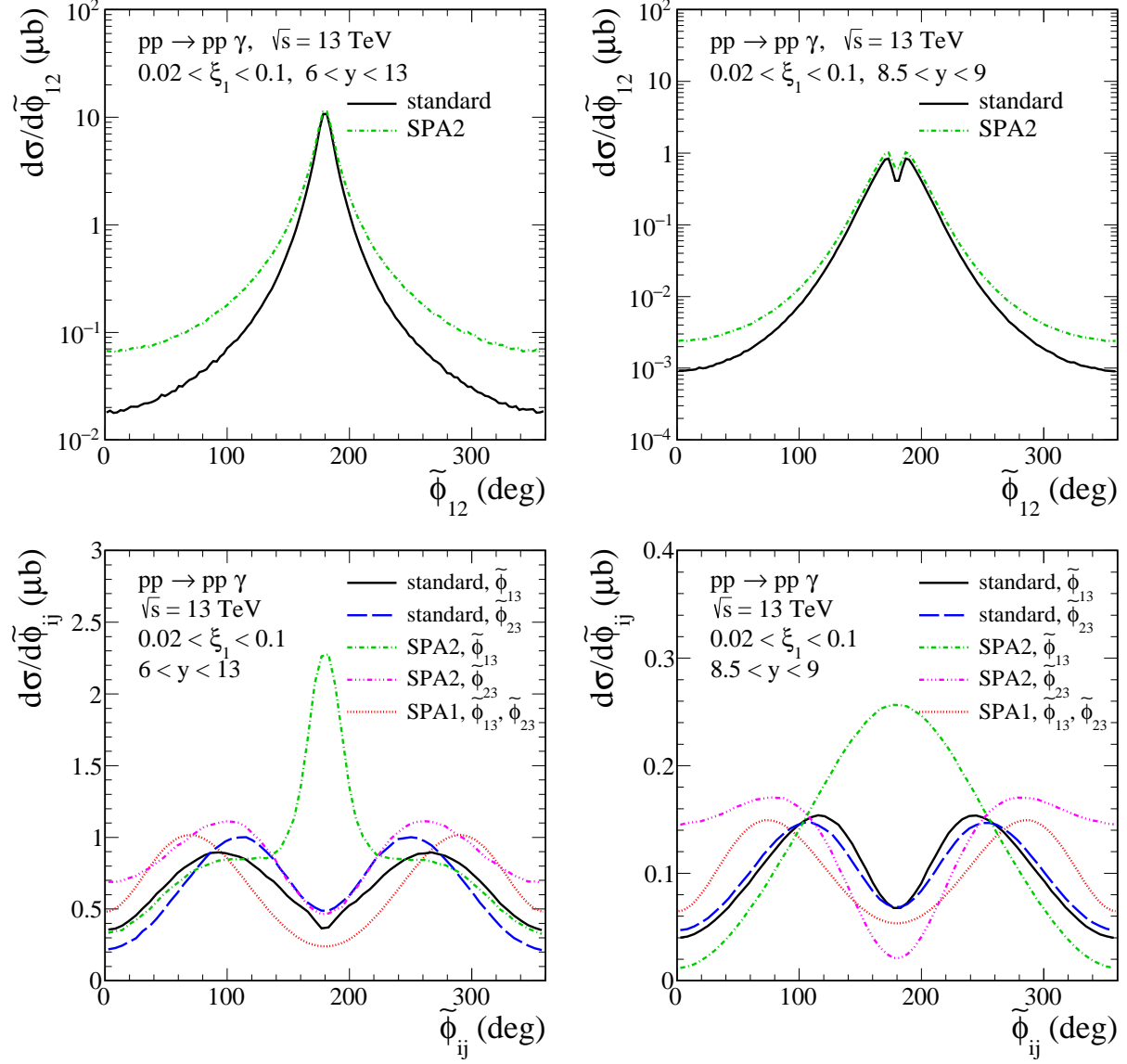


FIG. 7. The distributions in the angles  $\tilde{\phi}_{ij}$  defined by (3.3) for the  $pp \rightarrow pp\gamma$  reaction calculated for  $\sqrt{s} = 13$  TeV,  $0.02 < \xi_1 < 0.1$ ,  $6 < y < 13$  (left panel), and  $8.5 < y < 9$  (right panel). The results for the standard bremsstrahlung model and the SPAs are shown.

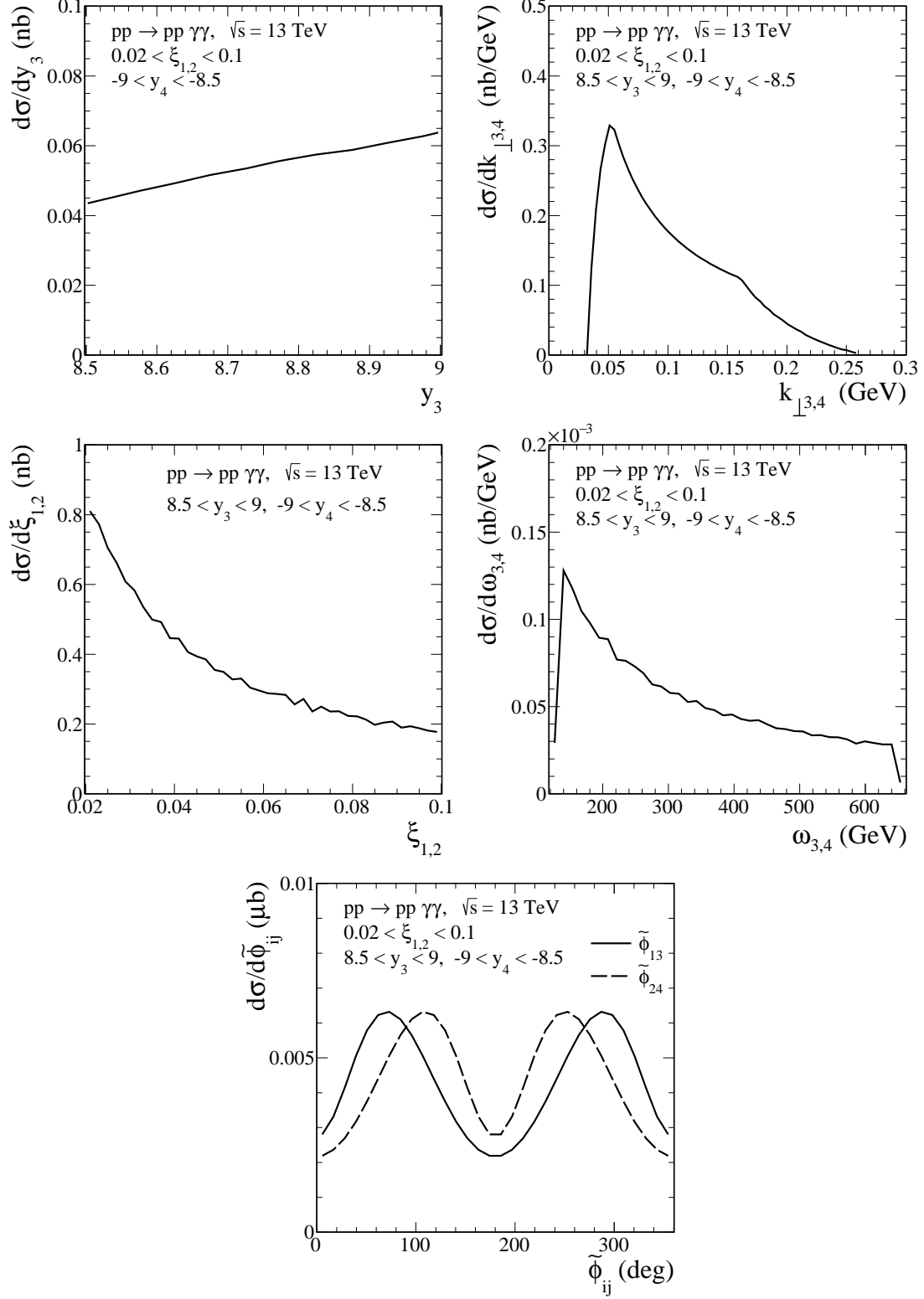


FIG. 8. The distributions for the two-photon bremsstrahlung in the  $pp \rightarrow pp\gamma\gamma$  reaction. The calculations were done for  $\sqrt{s} = 13$  TeV,  $8.5 < y_3 < 9$ ,  $-9 < y_4 < -8.5$ , and  $0.02 < \xi_{1,2} < 0.1$ . Shown are results for SPA1.

## IV. CONCLUSIONS

In this paper we have studied single- and double-photon bremsstrahlung at very-forward and backward photon rapidities in proton-proton collisions at high c.m. energies. To calculate the amplitudes of the reactions  $pp \rightarrow pp\gamma$  and  $pp \rightarrow pp\gamma\gamma$  the framework of the tensor-pomeron model was used.

We have started our analysis with the reaction  $pp \rightarrow pp\gamma$ , single photon production. We have compared our standard bremsstrahlung results, which we called also “exact” results, and the results using the approximations SPA1 and SPA2. These approaches were discussed in our previous paper [17] but in a different kinematic region. In the present paper, we have shown that in the forward-rapidity region and for  $0.02 < \xi_1 < 0.1$  (that corresponds to  $120 \text{ GeV} < \omega < 660 \text{ GeV}$ ) the standard results and the SPA1 results for purely photonic distributions ( $d\sigma/dk_\perp$ ,  $d\sigma/d\omega$ ,  $d\sigma/dy$ ) are very close to each other, while the SPA2 overestimates differential cross sections; see Fig. 2 and Fig. 5.

We have studied the azimuthal angle correlations between outgoing particles (see Fig. 7). We observe very interesting correlations between protons and photons. Moreover, these correlations are significantly different for our “exact” approach and for the SPA1 and SPA2 approaches. Therefore, we emphasize that for detailed comparisons of our predictions with experiment and in order to distinguish our “exact” and the approximate approaches measurement of the outgoing protons would be most welcome, if not indispensable.

We have estimated the coincidence cross section for two-photon bremsstrahlung in the  $pp \rightarrow pp\gamma\gamma$  reaction within the SPA1 approach. We have required that the final state protons and photons can be measured by the ATLAS forward proton spectrometers (AFP) and LHCf detectors, respectively. We have imposed the kinematical cuts  $8.5 < y_3 < 9$ ,  $-9 < y_4 < -8.5$ ,  $0.02 < \xi_{1,2} < 0.1$ , and obtained the corresponding cross section  $\sigma \simeq 0.03 \text{ nb}$  for  $\sqrt{s} = 13 \text{ TeV}$ . Our predictions can be verified by the ATLAS-LHCf measurement. In the future possible backgrounds to the bremsstrahlung contributions must be evaluated in order to confirm the feasibility of the bremsstrahlung measurement.

Let us finally comment on experimental signatures for our processes. The single photon bremsstrahlung mechanism should be identifiable by the measurement of proton and photon on one side and by checking the exclusivity condition (no particles in the main detector) without explicit measurement of the opposite side proton by AFP. Whether this is sufficient requires further studies, since such a measurement will probably include one-side diffractive dissociation, which can be of the order of 20-30 %. The cross section for two photons on different sides is rather small but should be measurable. Here a study of the background contributions should be done.

## ACKNOWLEDGMENTS

We are very much indebted to Oldrich Kepka for useful discussions on the possible ATLAS-LHCf measurement, using AFP and LHCf detectors on one and both sides of the ATLAS interaction point. This work was partially supported by the Polish National

- [1] O. Scholten and A. Y. Korchin, *Virtual-pion and two-photon production in pp scattering*, Phys. Rev. C **65** (2002) 054004, arXiv:nucl-th/0203078.
- [2] H. Haberzettl and K. Nakayama, *Gauge-invariant formulation of  $NN \rightarrow NN\gamma$* , Phys.Rev. **C85** (2012) 064001, arXiv:1011.1927 [nucl-th].
- [3] A. Y. Korchin and O. Scholten, *Dilepton production in nucleon-nucleon collisions and the low-energy theorem*, Nucl. Phys. A **581** (1995) 493.
- [4] A. Y. Korchin, O. Scholten, and D. van Neck, *Low-energy theorems for virtual nucleon-nucleon bremsstrahlung; formalism and results*, Nucl. Phys. A **602** (1996) 423.
- [5] J. Chwastowski, L. Fulek, R. Kycia, R. Sikora, J. Turnau, A. Cyz, and B. Pawlik, *Feasibility Studies of Exclusive Diffractive Bremsstrahlung Measurement at RHIC Energies*, Acta Phys. Polon. B **46** no. 10, (2015) 1979, arXiv:1501.06264 [hep-ex].
- [6] J. J. Chwastowski, S. Czekierda, R. Kycia, R. Staszewski, J. Turnau, and M. Trzebiński, *Feasibility studies of the diffractive bremsstrahlung measurement at the LHC*, Eur. Phys. J. C **76** no. 6, (2016) 354, arXiv:1603.06449 [hep-ex].
- [7] J. J. Chwastowski, S. Czekierda, R. Staszewski, and M. Trzebiński, *Diffractive bremsstrahlung at high- $\beta^*$  LHC*, Eur. Phys. J. C **77** no. 4, (2017) 216, arXiv:1612.06066 [hep-ex].
- [8] O. Adriani *et al.*, *Measurement of forward photon production cross-section in pp collisions at  $\sqrt{s} = 510$  GeV with RHICf detector*, arXiv:2203.15416 [hep-ex].
- [9] O. Adriani *et al.*, (LHCf Collaboration), *Measurement of zero degree inclusive photon energy spectra for  $\sqrt{s} = 900$  GeV proton-proton collisions at LHC*, Phys. Lett. B **715** (2012) 298, arXiv:1207.7183 [hep-ex].
- [10] O. Adriani *et al.*, (LHCf Collaboration), *Measurement of zero degree single photon energy spectra for  $\sqrt{s} = 7$  TeV proton-proton collisions at LHC*, Phys. Lett. B **703** (2011) 128, arXiv:1104.5294 [hep-ex].
- [11] O. Adriani *et al.*, (LHCf Collaboration), *Measurement of forward photon production cross-section in proton-proton collisions at  $\sqrt{s} = 13$  TeV with the LHCf detector*, Phys. Lett. B **780** (2018) 233, arXiv:1703.07678 [hep-ex].
- [12] (ATLAS Collaboration), *Measurement of contributions of diffractive processes to forward photon spectra in pp collisions at  $\sqrt{s} = 13$  TeV*, ATLAS-CONF-2017-075.
- [13] A. Tiberio *et al.*, *LHCf Run II physics results in proton-proton collisions at  $\sqrt{s} = 13$  TeV*, PoS **ICHEP2022** (2022) 121.
- [14] H. Menjo *et al.*, (on behalf of the LHCf and RHICf Collaboration), *Status and Prospects of the LHCf and RHICf experiments*, PoS **ICRC2021** (2022) 301.
- [15] C. Ewerz, M. Maniatis, and O. Nachtmann, *A Model for Soft High-Energy Scattering: Tensor Pomeron and Vector Odderon*, Annals Phys. **342** (2014) 31, arXiv:1309.3478 [hep-ph].
- [16] P. Lebiedowicz, O. Nachtmann, and A. Szczurek, *High-energy  $\pi\pi$  scattering without and with photon radiation*, Phys. Rev. D **105** no. 1, (2022) 014022, arXiv:2107.10829 [hep-ph].
- [17] P. Lebiedowicz, O. Nachtmann, and A. Szczurek, *Soft-photon radiation in high-energy proton-proton collisions within the tensor-Pomeron approach: Bremsstrahlung*, Phys. Rev. D **106** no. 3, (2022) 034023, arXiv:2206.03411 [hep-ph].
- [18] P. Lebiedowicz, O. Nachtmann, and A. Szczurek, *Central exclusive diffractive production of single photon in high-energy proton-proton collisions within the tensor-pomeron approach*,

- arXiv:2302.07192 [hep-ph].
- [19] V. A. Khoze, J. W. Lamsa, R. Orava, and M. G. Ryskin, *Forward physics at the LHC: detecting elastic  $pp$  scattering by radiative photons*, JINST **6** (2011) P01005, arXiv:1007.3721 [hep-ph].
  - [20] P. Lebiedowicz and A. Szczurek, *Exclusive diffractive photon bremsstrahlung at the LHC*, Phys.Rev. **D87** (2013) 114013, arXiv:1302.4346 [hep-ph].
  - [21] V. A. Khoze, A. D. Martin, and M. G. Ryskin, *Can invisible objects be ‘seen’ via forward proton detectors at the LHC?*, J. Phys. G **44** no. 5, (2017) 055002, arXiv:1702.05023 [hep-ph].
  - [22] A. Cisek, P. Lebiedowicz, W. Schafer, and A. Szczurek, *Exclusive production of  $\omega$  meson in proton-proton collisions at high energies*, Phys.Rev. **D83** (2011) 114004, arXiv:1101.4874 [hep-ph].
  - [23] P. Lebiedowicz and A. Szczurek, *Exclusive  $pp \rightarrow pp\pi^0$  reaction at high energies*, Phys. Rev. **D87** (2013) 074037, arXiv:1303.2882 [hep-ph].
  - [24] S. Foroughi-Abari and A. Ritz, *Dark sector production via proton bremsstrahlung*, Phys. Rev. D **105** no. 9, (2022) 095045, arXiv:2108.05900 [hep-ph].
  - [25] J. L. Feng *et al.*, *The Forward Physics Facility at the High-Luminosity LHC*, J. Phys. G **50** no. 3, (2023) 030501, arXiv:2203.05090 [hep-ex].
  - [26] M. Trzebinski, *Machine Optics Studies for the LHC Measurements*, Proc. SPIE Int. Soc. Opt. Eng. **9290** (2014) 929026, arXiv:1408.1836 [physics.acc-ph].